A Systematic Study of Isomorphically Substituted H-MAlPO-5 Materials for the Methanol-to-Hydrocarbons Reaction

UNIVERSITÀ DEGLI STUDI DI TORINO

A systematic study of isomorphically substituted H-MAlPO-5 materials for the methanol to hydrocarbons reaction

by

Magnus Morten, Lukasz Mentel, Andrea Lazzarini, Ilia A. Pankin, Carlo lamberti, Silvia Bordiga, Valentina Crocellà, Stian Svelle, Karl Petter Lillerud and Unni Olsbye

Chem. Phys. Chem **2017**, *18*, 1-13

DOI: 10.1002/cphc.201701024

A systematic study of isomorphically substituted H-MeAlPO-5 materials for the Methanol to Hydrocarbons (MTH) reaction

Magnus Mortén[a], Łukasz Mentel[a], Andrea Lazzarini[a], Ilia A. Pankin[b,c], Carlo Lamberti[b,c], Silvia Bordiga[b], Valentina Crocellà[b], Stian Svelle[a], Karl Petter Lillerud[a], Unni Olsbye[a]

[a]Centre for Materials Science and Nanotechnology, Department of Chemistry, University of Oslo, P.O. Box 1033, Blindern, N-0315 Oslo, Norway.

[b]Department of Chemistry, CrisDi Interdepartmental Centre and INSRM reference University of Turin, via Pietro Giuria 7, 10125 Turin, Italy.

[c]International Research Center "Smart Materials", Southern Federal University, Zorge Street 5, 344090 Rostov-on-Don, Russia.

ABSTRACT

Substituting metals for either aluminum or phosphorous in crystalline, microporous aluminophosphates creates Brønsted acid sites, well known to catalyze several key reactions, including the methanol to hydrocarbons reaction (MTH). In this work we have synthesized a series of metal-substituted aluminophosphates with AFI topology that differ primarily in acid strength and span a predicted range from high Brønsted acidity (H-MgAlPO-5, H-CoAlPO-5 and H-ZnAlPO-5), medium acidity (H-SAPO-5) and low acidity (H-TiAlPO-5, H-ZrAlPO-5). The synthesis was aimed to produce materials with homogenous properties (morphology, crystallite size, acid site density and surface area) in order to isolate the influence of metal substitution. This was verified by extensive characterization. The materials were tested in the MTH reaction at 450 °C using dimethyl ether (DME) as feed. A clear activity difference was found, where the predicted stronger acids converted DME significantly faster than the medium and weak Brønsted acidic materials. Furthermore, the stronger Brønsted acids (Mg, Co and Zn) produced more light alkenes than the weaker acids. The weaker acids, especially H-SAPO-5 produced more aromatics and alkanes, indicating that the relative rates of competing reactions change when decreasing acid strength.

Keywords: Methanol to Hydrocarbons, MTH, MTO, acid strength, zeotype, AlPO

1.0 Introduction

Controlled synthesis of advanced, functional materials at the nanoscale is now becoming achievable. However, decoupling individual material properties and assessing their influence on the material functionality remains a challenge.

For zeolites and zeotypes, a class of microporous aluminosilicates and aluminophosphates, control over material properties is already quite advanced. Extended research efforts devoted to finding procedures driving the synthesis towards materials with desired properties have

resulted in methodologies that allow control over particle size and morphology[1], [2], [3], [4] incorporation and distribution of active sites[5],[6] and construction of new topologies[7]. Moreover, the efforts are further stimulated by novel applications emerging to exploit the advanced material properties[8], [9].

The quest for linking structure and material properties to activity, "the materials genome", is ongoing, with the main challenge identifying the key properties of the materials [10]. By understanding and quantifying structure-activity relationships, a more rational approach to catalyst design is possible, improving existing and developing new processes. In surface science, considerable effort has been made to establish a descriptor based approach to transition-metal catalysis, linking measurable properties of the catalyst structure with activity and selectivity in catalyzed reactions [11], [12]. Control of material properties is thus of key importance in this quest, since it makes it possible to investigate the influence of the individual factors on the performance of the materials. The understanding gained from those investigations could subsequently be used in optimizing the performance of the materials for selected applications.

A particularly challenging process is the methanol to hydrocarbons reaction (MTH), where methanol or dimethyl ether (DME) are converted to larger hydrocarbons over a Brønsted acidic zeotype catalyst. Numerous studies have aimed to reveal how each of the material properties (catalyst composition, topology, morphology, crystal size and density of acid sites) can be optimized to improve conversion capacity, activity and product selectivity [13], [14].

The mechanism of MTH has been debated extensively with more than 20 unique mechanisms proposed to explain the initial carbon-carbon bond formation[13]. However, under steady state conditions Dahl and Kolboe proposed that reactions occur via a hydrocarbon pool mechanism where sequential methylation and elimination reactions occur on adsorbed carbon-species at the active site of the catalyst, co-catalyzing product formation [15], [16], [17]. Alkenes and aromatics constitute important adsorbed pool-species promoting two distinct product forming cycles (Scheme 1).

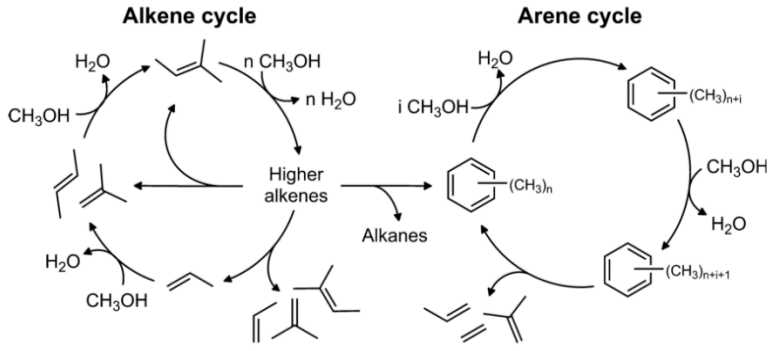

Scheme 1 General reaction scheme of the dual-cycle mechanism. Figure from [18]

In the alkene cycle, alkenes undergo methylation and cracking reactions, typically giving C_3 to C_5 alkenes as major products[19]. In the arene cycle, aromatics are methylated to substituted aromatics and undergo elimination reactions forming light alkenes and aromatics with fewer

substituents as products[20], [19b]. This latter reaction links the arene and alkene cycles. Another main reaction linking the two cycles is hydrogen transfer from either methanol or DME to an adjacent alkene, followed by addition of the dehydrogenated species to another alkene molecule, leading to diene formation. Subsequent cyclisation and hydrogen transfer reactions lead, finally, to the formation of aromatic products [21], [22], [23].

The active site of the MTH reaction is a Brønsted acid site (BAS). Although the fundamental aspects of solid Brønsted acidity are still under active investigations, there is an extensive literature covering experimental and computational approaches for constructing relative acid strength scales[24], [25]. Numerous approaches to quantify acidity have been suggested, using probe molecules, usually basic, in combination with an experimental probe detection technique. Examples include NH_3, CO, alcohols, nitriles and aromatic molecules, and common probe detection methods such as infrared spectroscopy, NMR and temperature programmed desorption with Mass Spectrometry[24], [25]. A computational alternative is the deprotonation energy (DPE) [26], [27] and NH_3 adsorption enthalpy [28], [29], that give a quantifiable ranking of acidity.

A few recent studies have addressed the influence of BAS strength on the MTH reaction. By using infrared spectroscopy and CO as a probe, the acidity difference of two isostructural zeolite/zeotype materials, H-SSZ-24 and H-SAPO-5, was established[18], [30]. The more acidic zeolite H-SSZ-24 produced more aromatics and C_2-C_3 hydrocarbons when feeding MeOH, while the weaker acidic H-SAPO-5 showed increased selectivity towards C_4-C_{6+} alkenes. It was concluded that the differences in product selectivity could be ascribed to the arene cycle being promoted over the more acidic material, while the alkene cycle was favored for the weaker acid[30]. More recently, a study in which methanol and dimethyl ether (DME) were compared as MTH feedstock provided additional insight in the matter. Importantly, it was found that methanol promotes hydrogen transfer reactions to a much higher extent than DME. Hence, the DME/methanol ratio in the reactor has substantial influence on product selectivity and catalyst conversion capacity. Furthermore, the study showed that the reversible methanol condensation reaction to DME and water was equilibrated over H-SAPO-5, but not over H-SSZ-24 under MTH reaction conditions [31]. This study shows that the difference in product selectivity observed for H-SSZ-24 and H-SAPO-5 could at least partly be ascribed to their different activity for the methanol condensation reaction, relative to subsequent methylation reactions.

The effect of BAS strength on a key MTH reaction step, olefin methylation, was explored computationally by Brogaard and Wang et al[29], [28], [32]. Ammonia adsorption enthalpy was identified as a descriptor for BAS strength over a series of metal-subsituted aluminophosphates, ranking the materials based on the BAS strength of the site created by isomorphic substitution. A scaling relationship for methylation rates of ethene and propene and BAS strength was established for several topologies and material compositions, yielding a predictive relationship for turnover frequencies of propene methylation based on the ammonia adsorption enthalpy on the BAS.

One of the investigated topologies, AFI, with unidimensional 12-ring channels (7.3Å x 7.3 Å), is ideal for experimental verification since it allows for bulky molecules to diffuse out of the structure, thereby limiting secondary reactions. In addition, since the discovery of AlPO-5 in 1982 by Wilson et al [33], numerous examples of compositional variants substituting heteroatoms in the structure have been reported, including the elements Mg, Zn, Co, Ti, Zr and Si[5], [34]. It has been debated whether isomorphic substitution of metals for either Al or P in the AFI structure, thereby creating a Brønsted acid site, is even possible[35]. However, several elements have been subject to rigorous study employing advanced spectroscopic techniques confirming framework incorporation [36]. Metal substituted AlPO-5 materials have been tested as catalysts in several reactions, including methanol to hydrocarbons[37], ethylation and propylation of aromatics[38], [39], cracking of alkanes[40] and aromatic isomerization[41].

In this work, we aim to study the effect of metal incorporation into the AlPO-5 structure and the effect of the created BAS on the MTH reaction. This will be a single parameter study attempted by synthesizing a series of metal substituted AlPO-5 materials with the same topology, similar crystal size, morphology and BAS density. The materials were extensively characterized to ensure that the catalyst lattices, including the immediate surroundings of the heteroatoms, were intact during testing. Furthermore, to avoid the influence of feed composition, DME was used as MTH feedstock instead of MeOH, keeping the DME/MeOH/H_2O ratio in the reactor similar across the materials. To the best of our knowledge, this is the first detailed, systematic study of metal substituted ALPO-5 materials used in the MTH reaction.

2.0 Materials and methods

2.1 Catalyst synthesis

H-MeAlPO-5 (Me = Mg, Co, Zn) were synthesized hydrothermally from water, triethylamine (TEA, Sigma Aldrich, 99%), orthophosphoric acid (VWR, 85%), Catapal B (Sasol) and $Mg(OAc)_2$ x 4 H_2O, $Co(OAc)_2$ x 4 H_2O, $Zn(OAc)_2$ x 4 H_2O, respectively (Sigma Aldrich, 99.99%). H-ZrAlPO-5 and H-TiAlPO-5 were synthesized from water, triethylamine, orthophosphoric acid (VWR, 85%), Catapal B (Sasol), Titanium (IV) isopropoxide (Sigma Aldrich, 97%) and Zirconium (IV) acetylacetonate (Sigma Aldrich, 97%), respectively.

For Mg, Co and Zn a representative gel composition of 1.0 Al_2O_3: 1.0 P_2O_5: 0.1 MeO: 1.0 TEA: 50 H_2O was made by stirring Catapal B in 80% of the total added water for 30 minutes, then adding the metal acetate dissolved in the remaining 20% of the water. Orthophoshoric acid was then added dropwise while stirring the solution, followed by dropwise addition of TEA. The solution was stirred for 30 minutes after addition of TEA and then crystallized for 4 h at 200 °C in a rotating Teflon lined steel autoclave. The total weight of the synthesis gel was typically 30 grams.

H-ZrAlPO-5 and H-TiAlPO-5 were made with a similar procedure, with the exception of adding Zirconium (IV) acetylacetonate and Titanium (IV) isopropoxide directly to the stirring solution of Catapal B and all of the added H_2O without dissolving the metal prior to the addition. AlPO-5 was made following the procedure without adding any metal to the Catapal B and H_2O solution.

The recovered material was washed and centrifuged three times with deionized water and dried at 80 °C for 18 h. Removal of TEA was performed by calcination in 20% O_2 in N_2 by heating to 550 °C (1 °C/min) and then 10 h at 550 °C.

2.2 Catalyst characterization

Temperature programmed desorption of *n*-propylamine was performed at atmospheric pressure in a fixed bed glass reactor (i.d. 11 mm), similar to the procedure described by Gorte et al [42]. The catalyst powder was pressed and sieved to 250 – 420 µm and pre-treated in a flow of air at 550 °C. The catalyst was then cooled to 150 °C. 80 ml/min of N_2 bubbled through a saturator containing *n*-propylamine at room temperature was then fed over the catalyst for 20 min. Excess *n*-propylamine was removed by flowing 80 mL/min of N_2 for 4 h at 150 °C. The temperature was then ramped at 20 °C/min up to 550 °C. The amount of propene desorbed quantified using an on-line Pfeiffer Omnistar quadrupole mass spectrometer.

Powder X-ray Diffraction (XRD) patterns for the as-synthesized and calcined catalysts were recorded using a Siemens Bruker D8 Discover instrument with Bragg–Brentano geometry using Cu K_α radiation (λ = 1.5406 Å).

The size and morphology of zeolite particles were analyzed with Scanning Electron Microscopy (SEM), recorded on a Hitachi SU 8230 FE-SERM. Utilizing Energy-dispersive X-ray Spectroscopy (EDS) with the same instrument, the elemental composition of the samples was determined.

The BET surface areas and pore volumes were determined using N_2 physisorption at 77 K using a Belsorp-mini II instrument. Fresh catalysts were outgassed under vacuum for 4 h, 1 h at 80 °C followed by a period of 3 h at 300 °C. The BET surface areas were determined based on a linear fit of the data in the p/p_0 range of 0.01 – 0.1.

FT−IR spectra were collected using a Bruker Vertex70 instrument equipped with a liquid nitrogen cooled MCT detector and a Harrick Praying Mantis accessory, able to collect data in Diffuse Reflectance mode (DRIFT). 128 spectra were averaged for each acquisition with a spectral resolution of 2 cm^{-1}. Data are reported in Log(R) vs. Wavenumber. The samples were activated in a 15 ml/min helium flow from RT to 450 °C (5 °C/min) in order to remove water, then cooled down to 70 °C to dose vapors of deuterated acetonitrile (CD_3CN, supplied by Sigma−Aldrich) as probe molecule, through a 15 ml/min helium flow. The desorption of the probe was performed by flowing pure helium (at the same conditions) for approximately 15 hours. CD_3CN has been used instead of CH_3CN to avoid the well−known

spectroscopic complication due to Fermi resonance between the ν(CN) vibration and the combination mode $\delta(CH_3) + \nu(CC)$.

X-ray absorption spectra at the Co and Zn K-edges were collected in transmission mode at the Swiss-Norwegian Beamline BM31[43], [44] of the European Synchrotron Radiation Facility (ESRF). A double crystal Si(111) monochromator in the continuous scanning mode was used to obtain monochromatic X-ray beam. Monochromator crystals were detuned to minimize the higher harmonic contribution. A third ionization chamber was used to measure the adsorption of the corresponding metal foil for internal energy calibration[45]. For H-ZnAlPO-5 samples EXAFS spectra in static conditions were collected up to k = 15.5 $Å^{-1}$, in a 15 min acquisition scan, while the sample activation was monitored collecting XANES each 3 min. Due to the lower Co content, for H-CoAlPO-5 samples EXAFS spectra where collected only up to k = 14.0 $Å^{-1}$, in a 30 min acquisition scan; XANES spectra were collected in 5 min. 3 and 5 equivalent EXAFS scan were collected for H-ZnAlPO-5 and H-CoAlPO-5, respectively, and averaged in k space before the EXAFS data analysis, as described elsewhere[46].

The measurements were performed in *operando* mode using a microtomo reaction cell (hosting the sample in form of self-supported pellet) that allows sample temperature and gas flows to be remotely controlled and that allows the gas outlet to be analyzed by Pfeiffer Omnistar Mass Spectrometer (MS)[47], [48], [49]. For H-CoAlPO-5 and H-ZnAlPO-5 the following protocol was followed: (1) sample activation by heating RT to 550 ℃ in air (5 °C/min), monitored by XANES. (2) Subsequent cooling in He flow till 450 ℃ (EXAFS collection). (3) The reaction gas feed (2 mL/min helium sent through a saturator containing MeOH at room temperature) was sent directly through the microtomo cell (hereafter named 1st cycle) (EXAFS collection after stabilization, monitored by online MS). (4) He was flushed at 450 °C for 2 hours. (5) The reaction gas feed (CH_3OH + He) was then sent to a reactor loaded with a commercial zeolite H-ZSM-5 sample (ZeoChem, Si/Al = 59) to convert the methanol to hydrocarbons, which subsequently was sent to the sample cell in order to mimic high conversion over the samples (2nd cycle). Also for step (5) the EXAFS collection started after stabilization, monitored by online MS.

2.3 Catalytic testing

Catalytic tests were performed at atmospheric pressure in fixed bed quartz reactors with the catalyst powder pressed and sieved to 250 – 420 μm. The inner diameter of the reactor was 8 mm. Reaction temperature was monitored by a thermocouple protected by a 3 mm wide quartz sleeve inserted into the middle of the catalyst bed. Dimethyl ether (Praxair or AGA, 25 mol% DME/Argon 6.0) was used as reactant. A range of space velocities was obtained by simultaneously adjusting the flow of the reactant line and a second gas line with pure helium. The catalysts were activated with an initial heating ramp 5 °C/min under 20% O_2 in helium to 550 °C, and the temperature was kept for 1 h under 100% O_2. Then, the catalysts were cooled to reaction temperature at 5 °C/min under helium flow.

The catalysts were tested in two sets of experiments. In the first experimental regime for determining DME conversion activity at 450 °C, ~40 mg of catalyst was used under a total flow of reactants and inert gas at 50 mL/min with p_{DME} =13 mbar. This gave a space velocity of 1.9 h^{-1}. In the second experimental regime in order to obtain comparable selectivity data at 450 °C, catalyst mass was varied under a fixed total flow reactant and inert gas of 50 mL/min and p_{DME} = 13 mbar. This gave space velocities of 1.9 (H-MgAlPO-5), 1.1 (H-CoAlPO-5), 0.8 (H-ZnAlPO-5), 0.47 (H-SAPO-5), 0.23 (H-ZrAlPO-5), 0.70 (H-TiAlPO-5) and 0.25 (AlPO-5) $g_{DME} \cdot g_{cat}^{-1} h^{-1}$.

The effluent from the reactor was analyzed after 5 min of reaction, and subsequently, every 75 minutes, by an on-line GC/MS instrument (Agilent 7890 with flame ionization detector and 5975C MS detector) using two Restek Rtx-DHA-150 columns. Hydrogen (Praxair, purity 6.0) was used as carrier gas.

3.0 Results and discussion

3.1 Synthesis and catalyst characterization

A summary of obtained characterization data including the size of the particles (from SEM micrographs), specific surface area (from BET), acid site density estimated from *n*-propylamine TPD and the heteroatom content based on EDS measurements, for all synthesized materials can be found in Table 1.

Table 1 Key material characteristics for synthesized H-MeAlPO-5 materials

Material	**Crystal Size (µm)**	**BET (m^2/g)**	**Acid site density (mmol/g)[a]**	**Density of Me (mmol/g)[b]**
H-MgAlPO-5	1 x 2.5	360	0.102	0.1
H-ZnAlPO-5	1 x 2.5	362	0.094	0.2
H-CoAlPO-5	1.5 x 2	347	0.081	0.2
H-SAPO-5[c]	1 x 2	340	0.068	0.3
H-ZrAlPO-5	2 x 4.5	352	0.065	-[d]
H-TiAlPO-5	3.5 x 3	329	0.060	0.2
AlPO-5	1 x 1	370	n.a.	-[e]

[a]Determined by *n*-propylamine TPD [b]Estimated from EDS, based on ratio of Me and either Al or P [c]See ref [50] [d]Overlap between Zr/P peaks, no estimate obtained. [e]No heteroatom detected by EDS

X-ray diffractograms were measured for the as-synthesized (Supporting Information, S1) and calcined materials (Figure 1). All materials were highly crystalline and showed AFI structure as the only phase present. The materials were stable up to 550 °C during calcination, and showed no sign of degradation after heating, evident from the XRD diffractograms of the calcined samples (Figure 1).

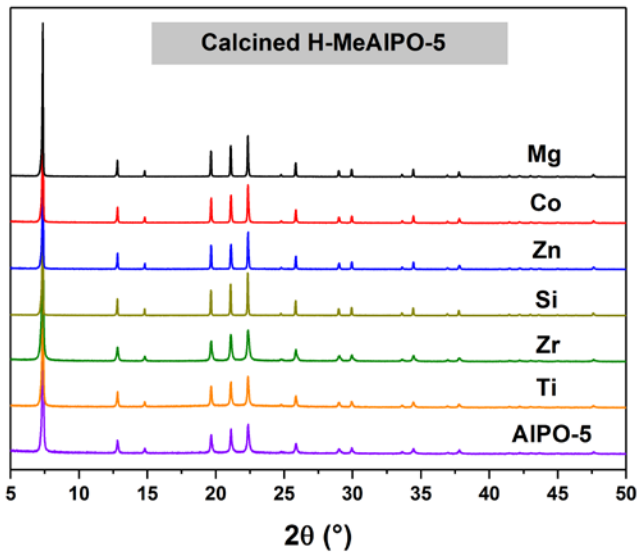

Figure 1 XRD powder patterns of the calcined H-MeAlPO-5 materials and AlPO-5 used in this work (See supporting Information S1 for XRD powder patterns for as-synthesized samples).

The BET areas of the samples were determined to be between 329 m^2/g and 362 m^2/g, with H-TiAlPO-5 and H-ZnAlPO-5 being the two extremes of the metal-substituted series. The non-substituted AlPO-5 showed a higher slightly surface area of 370 m^2/g (Table 1). These results indicate that little pore blocking due to extra framework metal-species is occurring.

Representative SEM micrographs (Figure 2) show the hexagonal barrel-shaped morphology of the samples. The crystallites have a homogenous size distribution with typical averages between 1 – 2 μm in diameter and 2 – 3 μm along the c-axis. H-ZrAlPO-5 and H-TiAlPO-5 showed slightly larger crystallites, with averages from 2 – 4 μm in diameter and 3 – 5 μm along the c-axis. The morphology of both samples resembled hexagonal barrels, but with less well defined edges compared to the rest of the synthesized materials.

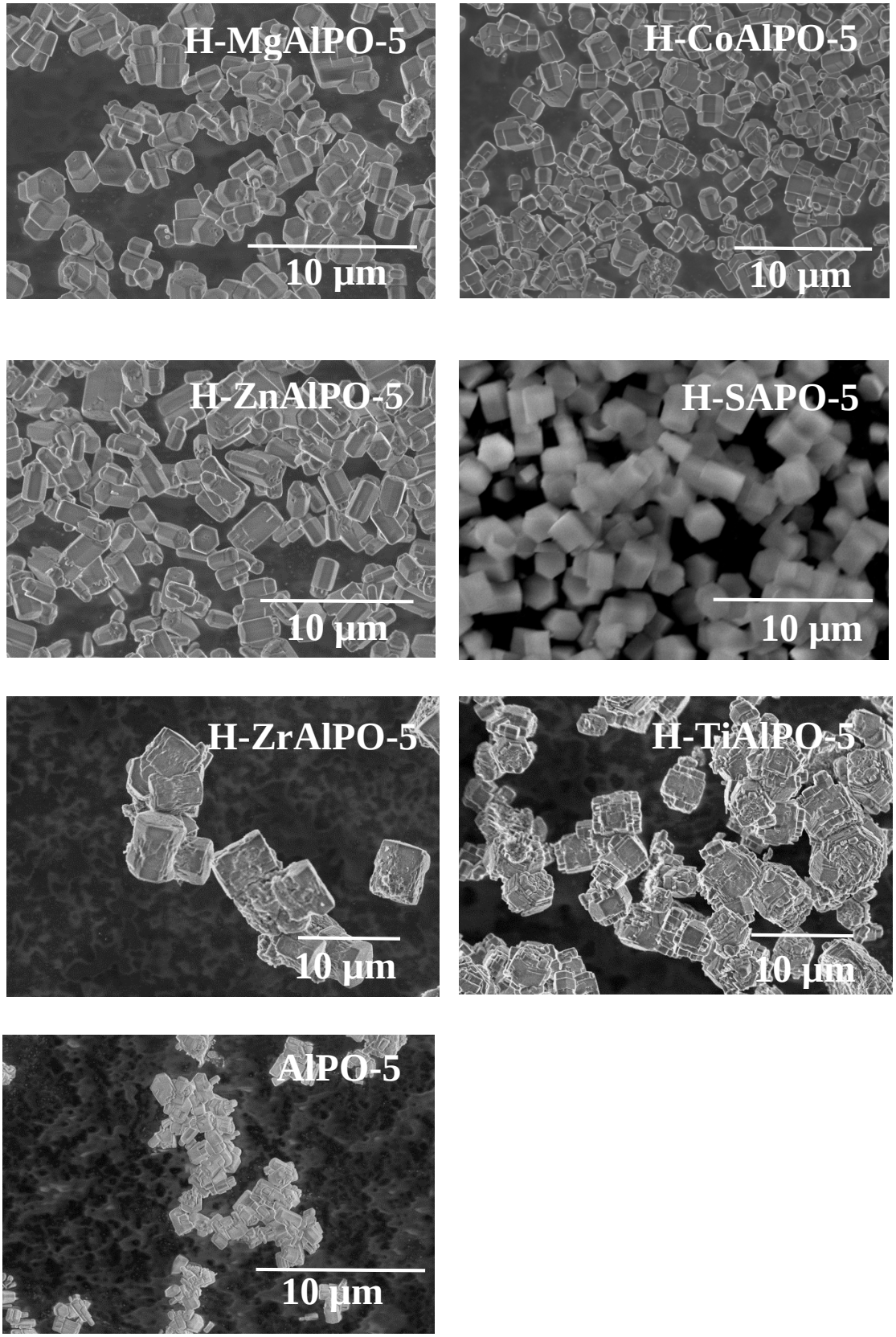

Figure 2 SEM micrographs of H-MeAlPO-5 materials and AlPO-5.

n-Propylamine TPD was used to probe Brønsted acidity and quantify the density of Brønsted acid sites. The desired density of Brønsted acid sites was 0.1 mmol/g, a value that has previously been reported for most of the materials synthesized in this work[37], [51]. Table 1 show that the density of acid sites varied somewhat between the +2 and +4 metals. For the +4 metals the density of acid sites was lower than for +2 metals, ranging from 0.060 mmol/g, 0.065 mmol/g and 0.068 mmol/g for H-TiAlPO-5, H-ZrAlPO-5 and H-SAPO-5, respectively. This is in agreement with + 4 metals being less likely to substitute into the framework since P-O bonds are more covalent in character than Al-O bonds in the ALPO-5 framework[52]. For the +2 metals the density of acid sites varied from 0.081 mmol/g, 0.094 mmol/g and 0.102mmol/g for H-CoAlPO-5, H-ZnAlPO-5 and H-MgAlPO-5, respectively. To investigate the effect of varying acid site density on the MTH reaction, experiments with a higher density sample (Mg) and lower density sample (Zn) were performed (Supporting Information, S2). The product selectivities did not vary significantly between the high and low density samples under these conditions, so it was concluded that the variation in acid site density between the samples was satisfactory for the present study.

The estimates of metal content from EDS provide complementary information to the density of Brønsted acid sites obtained from *n*-propylamine TPD, from which we can infer the amount of metal present in the sample that was not incorporated into the lattice as BAS. As can be seen in Table 1, the total density of metals varied somewhat between the samples, ranging from 0.1 to 0.2 mmol/g for the materials synthesized in this work. The rough agreement between the samples is expected, since the same synthetic procedure was followed, adding the same amount of metal salts to the synthesis gel. The excess metal can exists as a variety of species that are hard to precisely identify, however except for the H-SAPO sample the amounts of those species are small.

A direct evidence of metal incorporation into the AlPO-5 framework and the consequent formation of strong Brønsted acid sites were assessed through IR spectroscopy. Due to the prohibitive particle dimensions in transmission measurements, the samples were studied in reflectance mode (see Experimental section). Figure 3 shows the spectra collected after sample activation at 450 °C under helium flow for the full set of samples.

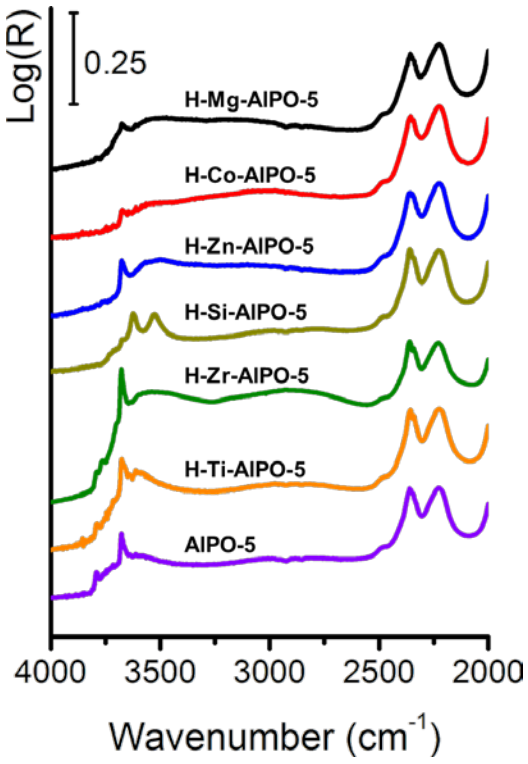

Figure 3 DRIFT spectra of AlPO-5 and H-MeAlPO-5 after activation at 450 °C in He. The spectra were collected at 120 °C in order to avoid moisture contamination and water adsorption.

As already described, the IR spectra of the H-MeAlPO-5 materials (AFI topology) are characterized by strong bands in the region below 2500 cm^{-1}, which are assigned to overtone and combination vibrations of the lattice. Above 2500 cm^{-1}, absorption bands attributed to the stretching vibrations of hydroxyl groups are observed[53]. In all spectra, a characteristic band at 3674 cm^{-1} ascribed to the terminal P-OH groups was present. Moreover in H-SAPO-5 and AlPO-5 the respective bands for Si-OH and Al-OH terminal groups were present at 3790 and 3735 cm^{-1}. The only sample that shows well defined maxima ascribable to bridging Brønsted sites is H-SAPO-5 (3625 cm^{-1}), while other H-MeAlPO-5 materials are characterized by a continuum in the spectra profile, suggesting that the OH group is engaged in hydrogen bonding[37]. All these OH species in the spectral region below 3650 cm^{-1} are usually ascribed to OH bonds presenting Brønsted acidity, as reported in the literature for these materials[54].

In order to investigate the nature of the acid sites in more detail, selected samples (Mg, Co, Si and pure AlPO-5) were studied using CD_3CN as a probe molecule (see Supporting information S3). All the samples analyzed exhibit the following spectral features: i) a broad band centered at 2310-2315 cm^{-1}, ascribed to the probe adsorbed on Al^{3+} Lewis acid site; ii) a sharp band at 2263 cm^{-1}, due to physisorbed CD_3CN; iii) a band between 2285 and 2275 cm^{-1} which is assigned to the probe adsorbed on terminal (phosphanols) and bridged hydroxyls groups (Brønsted sites); iv) the samples including Co^{2+} and Mg^{2+} show also a feature (well visible in the last desorption step - grey spectra in the insets) centered at 2301-2304 cm^{-1}, assigned to acetonitrile adsorbed on Lewis sites created by the incorporated Me^{2+} cations[54], [55]. These observations are in line with older literature, which showed that the AlPO-5 framework is so flexible that Al can interact with strong basic probes as a Lewis acid, without losing its tetrahedral lattice coordination[56]. The complexity of the IR spectra further

suggests that ranking of Brønsted acid strength for these materials must rely on theoretical predictions.

To sum up, the characterization data presented in this section show that the materials form a series with similar key properties such as particle size, morphology, surface area and acid site density. The materials differ in one respect, namely the nature of the isomorphically substituted heteroatom. This makes the series of materials well suited for a one-parameter variation study where the catalytic properties of the created Brønsted acid sites can be ascribed to differences in acid strength.

3.2 Catalytic testing

3.2.1 Catalytic activity of H-MeAlPO-5 materials at 450 °C in the MTH reaction

Although metal-substituted aluminophosphates have been studied extensively for over 30 years, there are only a few systematic studies where a consistent series of materials was examined to uncover the dependence of catalytic properties on the substituted element forming the BAS. In a pioneering studies on H-MeAlPO-5 materials with Me = Mg, Co, Zn, Si, Zr for MeOH conversion at 370 °C[37] Lischke et al found that H-SAPO-5 was the most active catalyst, followed by H-CoAlPO-5. H-MgAlPO-5 and H-ZnAlPO-5 was found to be significantly less active and H-ZrAlPO-5 showed negligible conversion. In an analogous study of H-SAPO-5 and H-CoAlPO-5, Popova et al reported that the initial conversion of MeOH was similar over the two materials at 450 °C[57].

In the present contribution, the Brønsted acidic H-MeAlPO-5 materials were designed to span a spectrum of acid strengths covering the high, medium and low values[32] while keeping properties such as particle size and morphology, density of acid sites maximally similar to a degree allowed by the synthetic procedure. The choice of the substituting elements was strongly influenced by the work of Brogaard and Wang et al where ammonia adsorption enthalpy was used as an acidity descriptor, establishing a ranking of the materials which correlated with rates of propene methylation[29], [28].

All synthesized H-MeAlPO-5 materials were tested as catalysts in the MTH reaction to evaluate catalytic activity. The MTH reaction is catalyzed by Brønsted acid sites and thus serves both as an indirect means of confirming framework incorporation of metals by demonstrating activity[35] and as a probe for the influence of the strength of the created BAS through the activities and selectivities across the materials. The H-MeAlPO-5 materials were tested at 450 °C and low feed rates (WHSV = 1.9 h^{-1}) and low DME partial pressure (13 mbar) to ensure catalytic activity across the series. Table 2 summarizes the activity of the catalysts expressed as initial turnover frequency (TOF) and initial conversion rate per gram of catalyst (r_{conv}). The theoretically calculated value for ammonia adsorption enthalpy is included in the table as an acid strength descriptor and serves as a theoretical ranking of the materials from strong to weak Brønsted acids. This ranking will be used throughout the discussion when addressing acid strength.

Before proceeding to the test results, it should be noted that the DME-to-Methanol ratio versus conversion graph in the reactor effluent was overlapping for all tested materials (Supporting Information S4), demonstrating that the activity and selectivity differences observed between the materials are not related to the relative abundance of DME, methanol and water in the reactor.

Table 2 H-MeAlPO-5 theoretical acidic strength (ΔE_{NH3}), turn-over frequency (TOF) and rate of DME conversion (r_{conv}) at 450 °C, p_{DME} = 13 mbar and WHSV = 1.9 h^{-1}.

Material	ΔE_{NH3} (kJ/mol)[a]	TOF ($mol_{prod} \cdot mol\ [H^+]^{-1} \cdot h^{-1}$)	r_{conv} ($10^{-2} \cdot mol_{prod} \cdot g_{cat}^{-1} \cdot h^{-1}$)
H-MgAlPO-5	-128	243	2.48
H-CoAlPO-5	-121	279	2.27
H-ZnAlPO-5	-119	217	2.04
H-SAPO-5	-83	118	0.80
H-ZrAlPO-5	-75	30	0.20
H-TiAlPO-5	-75	39	0.24
AlPO-5	-	-	0.13

[a]See Supporting Information S6

As can be seen in Table 2, the three most active catalysts were H-MgAlPO-5, H-CoAlPO-5 and H-ZnAlPO-5, with initial TOF being 243, 279 and 217 $mol_{prod} \cdot mol\ [H^+]^{-1} \cdot h^{-1}$, respectively. H-SAPO-5 gave an initial TOF of 118 $mol_{prod} \cdot mol\ [H^+]^{-1} \cdot h^{-1}$, a factor 2 smaller than the three strongest acids, while H-ZrAlPO-5 and H-TiAlPO-5 gave 30 and 39 $mol_{prod} \cdot mol\ [H^+]^{-1} \cdot h^{-1}$, respectively. The activity of the catalysts corresponds well with the theoretical acidity ranking based on ammonia adsorption enthalpy. This trend is in line with the scaling relation developed by Brogaard and Wang et al between NH_3 adsorption enthalpy and alkene methylation rate over H-MeAlPO-5 materials[32]. Furthermore, previous mechanistic studies point to a reaction between sorbed species as the rate-determining step of both hydrogen transfer reactions (leading to the first C-C bond formation, i.e.; to initiation of the MTH reaction) and alkene/arene methylation reactions (the propagation reactions of the dual-cycle MTH mechanism)[58], [59], [31]. The rate of such reactions generally increases with increasing coverage of the active site, which is in this case induced by a higher acid strength. The catalysts can be grouped, based both on their performance, measured by the theoretical acidity and initial TOF/r_{conv}, as high acidity/activity (Mg, Co, Zn) medium acidity/activity (Si) and low acidity/activity (Zr/Ti). This grouping coincides well with a grouping that can be made based on the chemical nature of the doping element. Mg, Co and Zn are formally +2 and are incorporated in place of Al atoms, Zr and Ti both have +4 oxidation state and substitute P lattice position the same as Si. However Si is the only metalloid in the +4 series and it is the most similar to P in size, which suggests that it will exert the smallest perturbation on the framework compared to Zr and Ti which are transition metals and have a larger ionic radii. The different behavior of +2 and +4 sites can be further rationalized in

view of the findings presented by Cora et al. where it was shown that AlPOs exhibit molecular-ionic character that is a consequence of being composed of Al^{3+} and PO_4^{3-} ions[52].

The unsubstituted AlPO-5 is also included in the series. Since it does not contain any Me-(OH)-P/Al bridge sites, it can serve as a benchmark for the low activity samples. Under the studied conditions, AlPO-5 showed conversion of DME to hydrocarbons, however at a lower rate than H-ZrAlPO-5 and H-TiAlPO-5 (0.13 vs. 0.20 and $0.24 \cdot 10^{-2} \cdot mol_{prod} \cdot g_{cat}^{-1} \cdot h^{-1}$). The conversion of DME over AlPO-5 may be ascribed to weakly acidic P-OH-groups. P-OH groups can catalyze dehydration of methanol to DME and at higher temperatures convert MeOH and DME to hydrocarbons[60]. To investigate the activity difference between H-ZrAlPO-5 and AlPO-5, a series of experiments were performed on the two materials and a physical mixture of ZrO and AlPO-5 (Supporting information S7). H-ZrAlPO-5 differed substantially in activity and product selectivity compared to AlPO-5 and the ZrO/AlPO-5 physical mixture. The significant activity difference between AlPO-5 and either of H-ZrAlPO-5 and H-TiAlPO-5 indicates that isomorphic substitution of Zr and Ti into the AlPO-5 framework is creating a Brønsted acid bridge site which alters the materials' catalytic properties. Overall, the MTH results show that the materials in this series have BAS with significant activity differences corresponding well with theoretical predictions of Brønsted acid strength.

3.2.2 Product selectivity

To investigate the influence of the different isomorphic substitutions into the AlPO-5 framework on product selectivity during the MTH reaction, the synthesized H-MeAlPO-5 materials were tested at 450 °C with variable feed rates (WHSV = 0.23 – 1.9 h^{-1}) in order to obtain comparable initial conversion levels. By reducing the feed rate, an initial conversion level of ~80% was obtained for H-MgAlPO-5, H-CoAlPO-5, H-ZnAlPO-5 and H-SAPO-5. For H-ZrAlPO-5 and H-TiAlPO-5 the highest conversion level obtained was 30 % and 12 %, respectively, employing very low feed rates (See Experimental section). Previous studies of the MTH reaction have shown that conversion-selectivity trends are often linear between 15 and 85% conversion, but differ widely for higher and lower conversion[61]. This is indeed what we observe for all materials except for H-TiAlPO-5, in case of which the conversion did not rise above 12% and therefore the H-TiAlPO-5 sample will not be included in the remainder of the discussion.

The conversion-selectivity results reported in Figures 4 to 8 were obtained during deactivation of the samples. This procedure was warranted by previous studies of H-SAPO-5 as MTH catalyst. They showed that the conversion-selectivity graphs were overlapping for fresh versus deactivated samples [50]. Additional tests performed in the present study over H-MgAlPO-5 at two different space velocities led to the same conclusion (Supporting Information S8).

The selectivity to three main categories of products, namely alkenes, alkanes and aromatics were chosen to illustrate the principal trends and highlight selectivity variations with heteroatom substitution (See Supporting information S5 for full set of selectivities).

Light alkenes, and propene in particular, are currently the target products of the majority of industrial MTH plants[61]. Figure 4A shows that the selectivity to alkenes for Mg, Co, Zn and Si was approximately constant, at a very high level (70-90 %), between 15 - 85% conversion, whereas for Zr it was steadily increasing towards 40% with increasing conversion. The most striking feature of alkene selectivity is the distinct behavior exhibited by material groups categorized according to predicted acid strength. The stronger Brønsted acidic materials (Mg, Co and Zn) gave significantly higher alkenes selectivity compared to the medium acidic H-SAPO-5. Weakly acidic H-ZrAlPO-5, gave the lowest alkene selectivity of the tested materials.

Moving on to alkane and aromatics selectivity (Figure 4, B and C), their selectivity trends were generally opposite to those of the alkenes. Their selectivity decreased from the weakest Brønsted acid H-ZrAlPO-5 to the strongest acid H-MgAlPO-5, with H-CoAlPO-5 slightly outside the general trend for alkanes (vide infra). In the MTH reaction scheme, alkanes and aromatics are typical products originating from hydrogen transfer reactions[13], [20]. The results presented in Figure 4 suggest that isomorphically substituting a metal into the aluminophosphate structure significantly alters the chemistry associated with the created Brønsted acid sites, shifting the product spectrum towards alkenes for the more acidic materials.

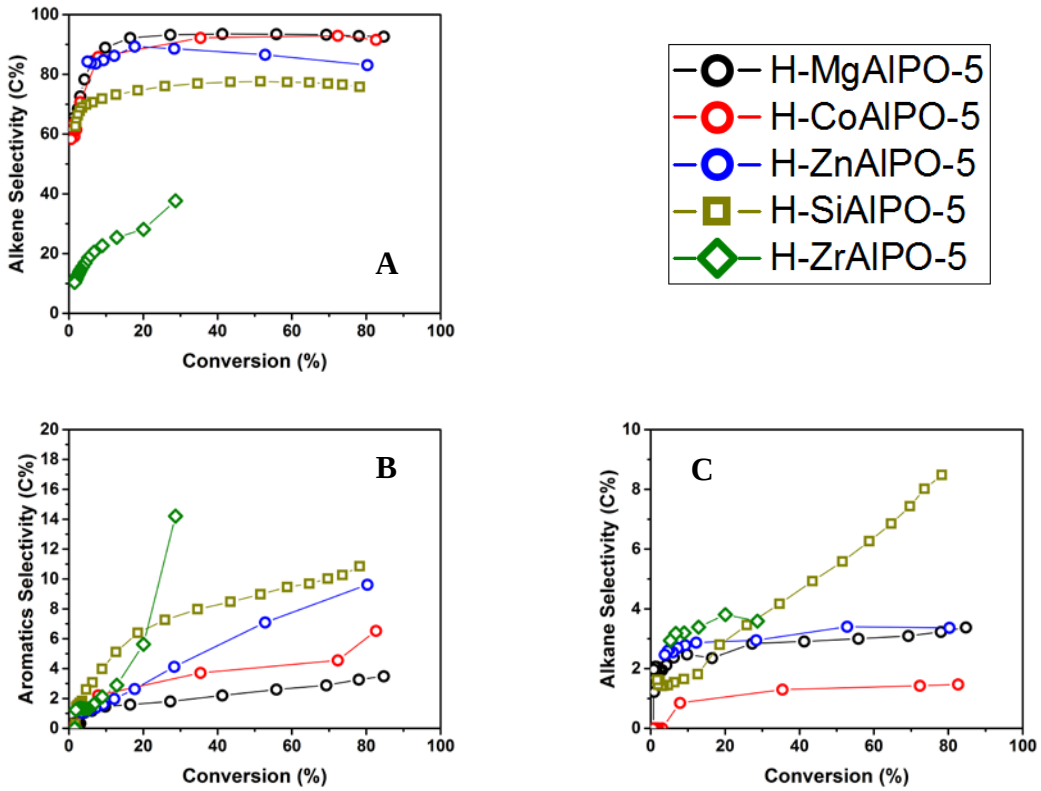

Figure 4 Product selectivty for DME conversion to three major product categories at 450 °C over the H-MeAlPO-5 materials. Alkenes include ethene, propene, butenes, pentenes and identified C_{6+} alkenes.

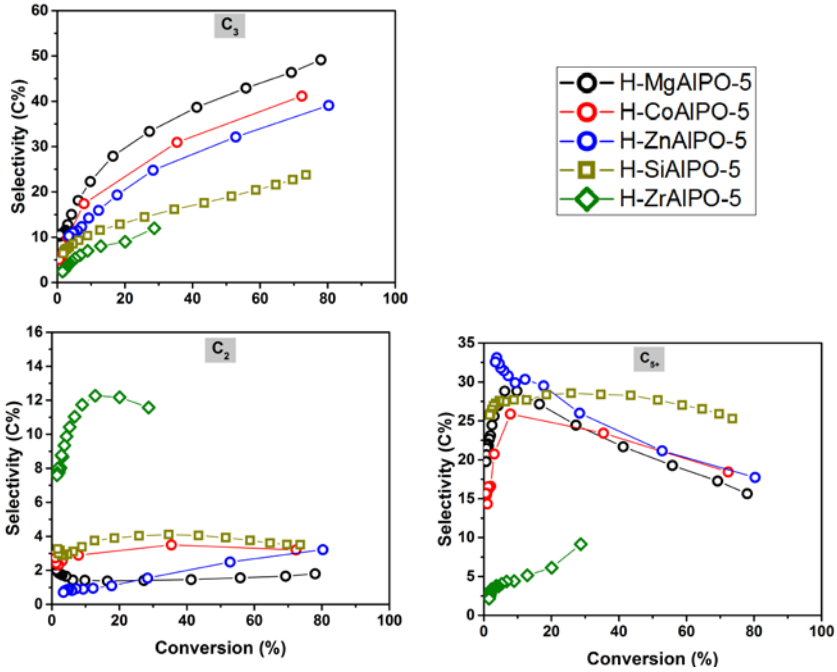

Figure 5 Product selectivty for DME conversion to C_3, C_2 and C_{5+} at 450 °C over the H-MeAlPO-5 materials.

Turning next to individual alkenes; ethene, propene and C_{5+} selectivity versus conversion for each material is shown in Figure 5. A striking observation in Figure 5A is the systematic increase in propene selectivity with increasing catalyst acid strength. At 75 % conversion, the selectivity to propene spanned a gap from 25 C% for H-SAPO-5 to almost 50 C% for H-MgAlPO-5. The difference in propene selectivity was significant also at lower conversion levels, ranging from 30 C% over H-MgAlPO-5, via 15 C% over H-SAPO-5 to 10 C% over H-ZrAlPO-5, all at 20% conversion. Another evident feature of the propene selectivity plot is the rapid increase in propene selectivity with increasing conversion. The slope of the curve is similar for the Mg-, Co- and Zn-containing materials, and somewhat lower for the Si- and Zr-containing materials. An opposite trend is observed for the C_{5+} alkenes (Figure 5B): Their selectivity decreased with increasing acid strength and with increasing conversion; the slope being steep and negative for the Mg-, Co- and Zn-containing materials, slightly negative for H-SAPO-5 and positive for H-ZrAlPO-5.

Alkenes are intermediate, autocatalytic species in the MTH reaction. Reactions leading to their formation and conversion include the methylation, oligomerization and cracking of short- and longer-chain alkenes, as well as dealkylation of aromatic compounds, in particular polymethylated benzene molecules [13], [20], [62], [30], [63]. The results presented in Figure 5 suggest that a high acid strength favors cracking of higher alkenes to form propene. This conclusion is in line with literature reports, which showed that only strongly acidic zeolites may crack C_{5+} alkenes to light C_2, C_3 alkenes, while less acidic zeotypes favored oligomerization followed by cracking to higher alkenes [64]. *[65]*. Interestingly, Lin et al. showed that 2-methyl-2-butene, as well as 1-pentene, were not cracked in monomolecular mechanism over H-SAPO-5, in line with the results presented in Figure 5. Furthermore, Meusinger et al studied cracking of *n*-hexane and *n*-butane over H-MgAlPO-5, H-CoAlPO-5 and H-SAPO-5[66]. The authors observed that comparable samples of the materials (acid site density, crystal size) gave a ranking based on TOF as H-MgAlPO-5 > H-CoAlPO-5 > H-SAPO-5. A comparison between the ethene and propene selectivity plots (Figure 5A and C) show that the two products have opposite trends with respect to selectivity versus predicted catalyst acid strength. This result suggests that the two products are formed via mechanistically distinct routes. Ethene formation has previously been assigned to polymethyl benzene dealkylation[13], [19a], [20], [67], although at higher temperatures, a parallel route to ethene from higher alkene cracking has been shown to increase in abundance over H-ZSM-5 zeolite[21]. Together, the results presented in Figures 4 and 5 may suggest that propene is mainly formed from the alkene cycle, while ethene is mainly formed from the arene cycle under the conditions used in this study (see Scheme 1). Furthermore, an increase in the predicted catalyst acid strength favors the alkene cycle over the arene cycle.

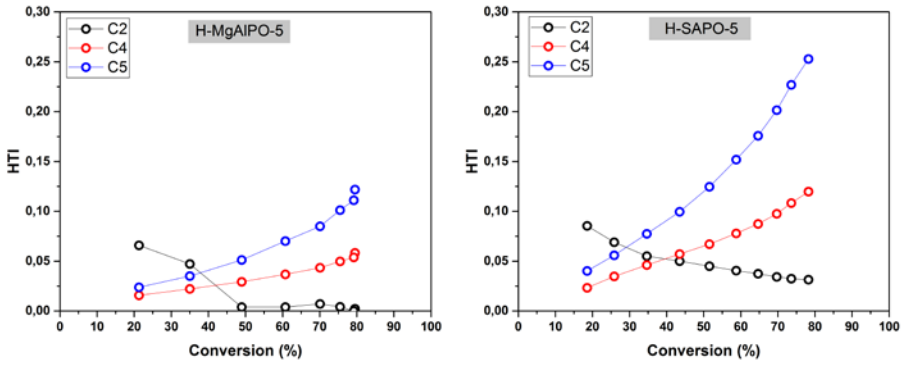

Figure 6 C_2, C_4 and C_5 HTI for H-MgAlPO-5 and H-SAPO-5 at 450 °C. HTI for C_3 was zero at all conversion levels and is not included in the figure.

The end products of hydrogen transfer reactions, i.e.; the alkanes, can be analyzed in view of the Hydrogen Transfer Index (HTI). HTI for C_2-C_5 products versus conversion over H-MgAlPO-5 and H-SAPO-5 is plotted in Figure 6. The two plots show that the HTI value observed for each individual alkane/alkene pair is higher for H-SAPO-5 than for H-MgAlPO-5. This result links the higher total alkene selectivity observed for the more acidic material of the two, H-MgAPO-5 (see Figure 4A), directly to the relative hydrogen transfer activity of the two materials. We further note that the HTI is zero for C_3, very low for C_2 (but increasing at decreasing conversion), and substantially higher for C_4 and C_5, over both materials. The difference between C_2, C_4 and C_5 is in line with what reported by Iglesia et al for H-Beta zeolite[68], and reflects the relative stability of primary versus secondary and tertiary carbocation intermediates. The zero HTI value observed for propene, when combined with the non-zero value observed for ethene, is surprising and cannot be explained at this point. However, we note that the same observation is made for both materials.

The mechanism of hydrogen transfer reactions in MTH has been scarcely studied, mainly due to the complexity of the product spectrum obtained even at low conversion (see e.g. [30]). Recently, however, studies in which methanol and DME were compared as methylating agent of benzene and isobutene, mainly over H-ZSM-5, yielded new insight in these reactions. Briefly, the studies revealed a key role of methanol and DME as hydrogen transfer agents between the alkene and arene cycles, as well as between monocyclic arenes and heavier analogues[59], [31]. Furthermore, hydrogen transfer reactions were found to take place at the Brønsted acid site, while isolated Lewis acid sites had negligible activity for both methylation and hydrogen transfer reactions[23]. The role of Lewis acid sites in MTH is still not fully revealed. Another recent study of MTH, using a H-ZSM-5 catalyst, reported that the rate of methanol conversion correlated with the number of Brønsted acid sites, while aromatics yield correlated with the number of Lewis acid sites in the material[21]. Although the underlying reason for this result is not fully understood, , the HTI results obtained suggest that the hydrogen transfer activity of H-MeAPO-5 is less influenced by Brønsted acid strength compared to other, competing reactions in the MTH reaction scheme.

Methane formation from two DME molecules via a methoxy methylene species was recently directly linked to the formation of the first C-C bond in the MTH reaction[58], [69]. Whereas such direct hydrogen transfer between two oxygenate molecules is feasible, the activation energy of this reaction is far higher than for hydrogen transfer from a DME or methanol molecule to an adjacent alkene molecule[59], [23]. Methane formation associated with the MTH initiation reaction is therefore assumed to take place mainly in the first part of the reactor, where the concentration of hydrocarbons is negligible[70]. Another pathway to methane formation is associated with hydrogen transfer from coke precursors to oxygenates, thereby forming polyaromatic molecules. This pathway becomes more abundant with increasing deactivation[71].

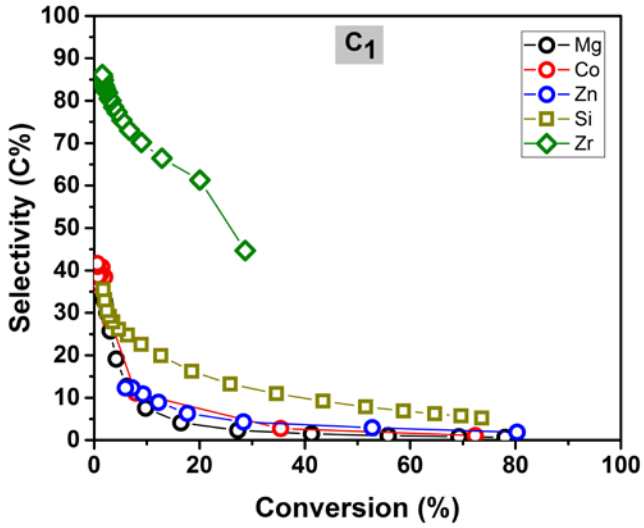

Figure 7 Methane selectivity over H-MeAlPO-5 materials at 450°C

Figure 7 shows the selectivity to methane over the H-MeAlPO-5 materials. In general, the selectivity to methane is low over the stronger Brønsted acidic materials, slightly higher over H-SAPO-5, and much higher over H-ZrAPO-5. At low conversion (< 15 %), the selectivity curves for the medium and strong acid materials converge to a common value. A deeper analysis of the methane formation rates is complicated by the different alkene selectivity over the studied materials. However, we note that the methane selectivity trends are in line with those obtained for the C_{2+} HTI, i.e.; that materials with low predicted acid strength favor hydrogen transfer reactions.

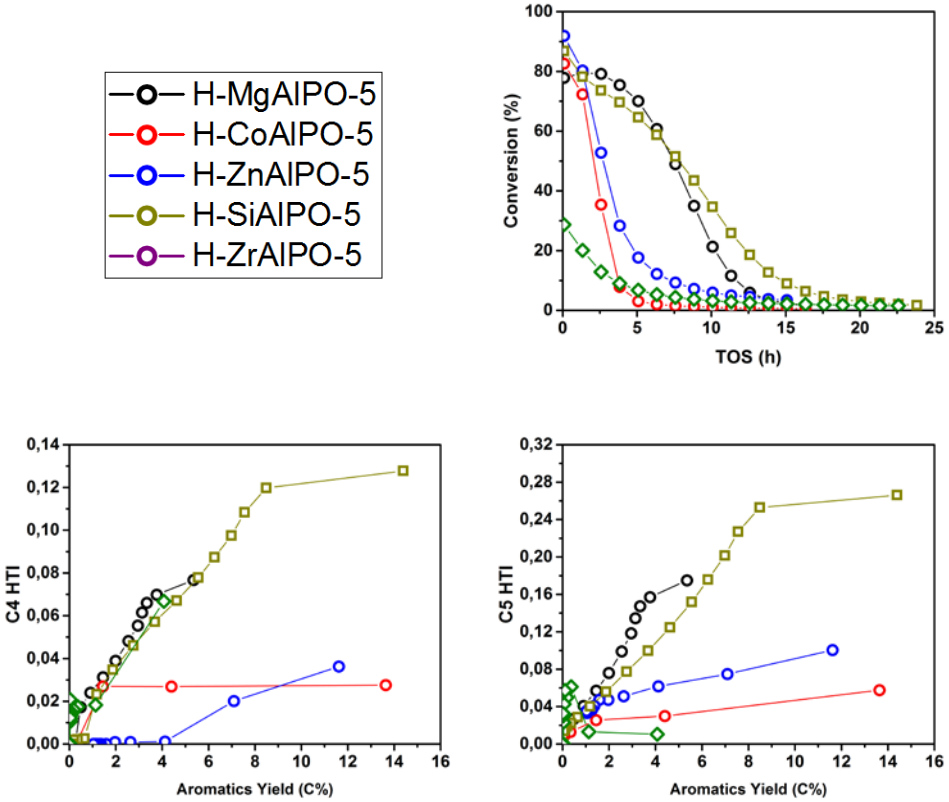

Figure 8 Deactivation plots and C_4/C_5 HTI versus Aromatic yield for DME conversion at 450 °C, pDME=13 mbar, WHSV = 0.23 – 1.9 h^{-1}.

Finally, we turn the attention to reactions leading to coke formation and deactivation of the catalysts. Conversion versus time on stream curves for all catalysts are shown in Figure 8, in addition to C_4 HTI and C_5 HTI versus aromatics yield plots. Considering first the Conversion versus Time on stream curves, it is interesting to note that among the materials with high acid strength (Mg-, Co-, Zn-substituted AlPO-5), which have very similar effluent product selectivity, the Co- and Zn-substituted materials deactivate much more rapidly than the Mg-containing material. Indeed, when considering the different WHSVs used in these tests, their DME conversion capacity is comparable to, or lower than, that of H-SAPO-5, which has substantially higher activity to hydrogen transfer products in the effluent than the more acidic materials (Figures 4, 6, 7). A possible explanation for this result could be leaking of Co and Zn from the H-MeAlPO-5 structure during testing. For this reason, in operando XAS measurements were performed for these two materials (Supporting information S9). Briefly, both Co and Zn were in the expected +2 oxidation state after calcination, and that the +2 oxidation state was retained during activation in air at 550 °C and more importantly during catalytic testing mimicking high and low conversion of DME/methanol (See Supporting information S9 for a detailed analysis). With the metal leaking hypothesis excluded, an alternative explanation was sought. In Figure 8, a clear, positive correlation between HTI and aromatics yield is observed for the Mg- and Si-containing materials, demonstrating that these products are formed by (oxygenate-promoted) hydrogen transfer reactions. In the Co- and Zn-containing materials, on the other hand, the HTI values are too low to account for the aromatics yield, suggesting another, parallel pathway to aromatics formation. Co- and Zn-

exchanged zeolites have previously been shown to have alkane dehydrogenation activity[72], [73], and we speculate that this is the case also for the isomorphically substituted H-CoAlPO-5 and H-ZnAlPO-5 materials used in this study. Such activity could contribute to more rapid deactivation of the Co- and Zn-containing catalysts.

Overall, the product selectivity data obtained over the isomorphically substituted H-MeAPO-5 materials strongly suggest that under the conditions used in this study, an increasing acid strength favours methylation and cracking reactions over hydrogen transfer reactions. Whereas the detailed interaction between reactant molecules and the active catalyst is not fully revealed, the study clearly shows that an increasing acid strength enhances the alkene versus the arene reaction cycle the total alkene selectivity, and the propene-to-ethene ratio of the H-MeAlPO-5 catalysts.

The MTH activity trend observed for the materials presented in this study are in line with those previously published by our group for two isostructural zeolite/SAPO pairs, i.e.; H-SSZ-13 versus H-SAPO-34 (CHA structure) and H-SSZ-24 versus H-SAPO-5 (AFI structure). In those contributions, the acid strength was assessed experimentally by the relative shift in the O-H stretch frequency of the Brønsted acid site upon CO adsorption, measured by IR spectroscopy. In both contributions, the material with highest acid strength, the zeolite, showed substantially higher activity for the MTH reaction than the corresponding SAPO material[74], [18]. The product selectivity trends could be reasonably assessed only for the H-SSZ-24 versus H-SAPO-5 pair, due to the diffusional restrictions of the H-SSZ-13 versus H-SAPO-34 pair. For H-SSZ-24 versus H-SAPO-5, the selectivity towards ethene and aromatic products was higher for H-SSZ-24 than for H-SAPO-5 when using methanol as feed [18], [31] while it was similar for the two materials when using DME as feed [31]. These results may seem disparate from those presented in the current contribution. However, taking into account the different properties of the material surrounding the active site in the more covalently bonded Si-O-Si zeolite lattice compared to the Al-O-P MeAlPO lattice, these results rather point to a more complex material-performance correlation than previously assessed.

4.0 Conclusion

Careful design and rigorous execution of the synthesis of a consistent series of isomorphically substituted H-MeAlPO-5 materials differing only by the substituted metal and homogenous with respect to the remaining properties allowed us to unambiguously attribute the observed differences in catalytic performance to acid strength associated with the modified BAS. Substantial characterization evidence was provided, firstly showing the homogeneity of the samples with respect to particle size, morphology, surface area and acid site density, and secondly strongly indicating the incorporation of the metals as BAS and their stability under reaction conditions. All materials were shown to be active in MTH at 450 °C with clear activity differences, agreeing well with the predicted acid strength.

The materials exhibit clear selectivity differences that can be categorized according to acid strength. Strong acids (Mg, Co, Zn), show the highest selectivity towards the desired alkene products, with a small selectivity towards alkanes and aromatic products. Medium strength acid (Si) shows an increased selectivity towards aromatics and alkanes while diminishing the proportion of alkenes. The weakly acidic Zr-substituted material follows the trend of decreasing alkene selectivity with decreasing acid strength.

These encouraging results will be pursued in future studies of individual reactions over the same series of catalysts.

Acknowledgement

The authors would like to thank Maria Mykland for synthesis of the AlPO-5 sample and Mustafa Kømurcu, Reynald Henry, Michael Dyballa for assistance during XAS measurements at the Swiss-Norwegian beamline at ESRF. Kirill A. Lomachenko and Aram L. Bugaev are acknowledged for fruitful discussion on the XAS data. The ESRF is acknowledged for granting beamtime at BM01.

M.M., L.M., A.L. and U.O. acknowledge the Norwegian Research Council for financial support through contract 239193.

IAP and CL acknowledge the Mega-grant of the Russian Federation Government to support scientific research at the Southern Federal University, No. 14.Y26.31.0001.

5.0 References

[1] Y. Tao, H. Kanoh, L. Abrams, K. Kaneko, *Chemical Reviews* **2006**, *106*, 896-910.

[2] K. Egeblad, C. H. Christensen, M. Kustova, C. H. Christensen, *Chemistry of Materials* **2008**, *20*, 946-960.

[3] M. Choi, K. Na, J. Kim, Y. Sakamoto, O. Terasaki, R. Ryoo, *Nature* **2009**, *461*, 246-249.

[4] Y. Seo, S. Lee, C. Jo, R. Ryoo, *Journal of the American Chemical Society* **2013**, *135*, 8806-8809.

[5] E. M. Flanigen, B. M. Lok, R. L. Patton, S. T. Wilson, in *Studies in Surface Science and Catalysis, Vol. Volume 28* (Eds.: A. I. Y. Murakami, J. W. Ward), Elsevier, **1986**, pp. 103-112.

[6] J. Li, A. Corma, J. Yu, *Chemical Society Reviews* **2015**, *44*, 7112-7127.

[7] W. J. Roth, P. Nachtigall, R. E. Morris, P. S. Wheatley, V. R. Seymour, S. E. Ashbrook, P. Chlubná, L. Grajciar, M. Položij, A. Zukal, O. Shvets, J. Čejka, *Nat Chem* **2013**, *5*, 628-633.

[8] A. Corma, *Journal of Catalysis* **2003**, *216*, 298-312.

[9] M. E. Davis, *Nature* **2002**, *417*, 813-821.

[10] J. K. Nørskov, T. Bligaard, *Angewandte Chemie International Edition* **2013**, *52*, 776-777.

[11] J. Greeley, T. F. Jaramillo, J. Bonde, I. Chorkendorff, J. K. Norskov, *Nat Mater* **2006**, *5*, 909-913.

[12] F. Studt, I. Sharafutdinov, F. Abild-Pedersen, C. F. Elkjær, J. S. Hummelshøj, S. Dahl, I. Chorkendorff, J. K. Nørskov, *Nat Chem* **2014**, *6*, 320-324.

[13] U. Olsbye, S. Svelle, M. Bjørgen, P. Beato, T. V. W. Janssens, F. Joensen, S. Bordiga, K. P. Lillerud, *Angewandte Chemie International Edition* **2012**, *51*, 5810-5831.

[14] M. Stöcker, *Microporous and Mesoporous Materials* **1999**, *29*, 3-48.

[15] I. M. Dahl, S. Kolboe, *Catalysis Letters* **1993**, *20*, 329-336.

[16] I. M. Dahl, S. Kolboe, *Journal of Catalysis* **1994**, *149*, 458-464.

[17] I. M. Dahl, S. Kolboe, *Journal of Catalysis* **1996**, *161*, 304-309.

[18] M. Westgård Erichsen, S. Svelle, U. Olsbye, *Catalysis Today* **2013**, *215*, 216-223.

[19] aS. Svelle, F. Joensen, J. Nerlov, U. Olsbye, K.-P. Lillerud, S. Kolboe, M. Bjørgen, *Journal of the American Chemical Society* **2006**, *128*, 14770-14771; bM. Bjørgen, S. Svelle, F. Joensen, J. Nerlov, S. Kolboe, F. Bonino, L. Palumbo, S. Bordiga, U. Olsbye, *Journal of Catalysis* **2007**, *249*, 195-207.

[20] S. Ilias, A. Bhan, *ACS Catalysis* **2012**, *3*, 18-31.

[21] S. Müller, Y. Liu, F. M. Kirchberger, M. Tonigold, M. Sanchez-Sanchez, J. A. Lercher, *Journal of the American Chemical Society* **2016**, *138*, 15994-16003.

[22] X. Sun, S. Mueller, Y. Liu, H. Shi, G. L. Haller, M. Sanchez-Sanchez, A. C. van Veen, J. A. Lercher, *Journal of Catalysis* **2014**, *317*, 185-197.

[23] J. S. Martínez-Espín, K. De Wispelaere, T. V. W. Janssens, S. Svelle, K. P. Lillerud, P. Beato, V. Van Speybroeck, U. Olsbye, *ACS Catalysis* **2017**, *7*, 5773-5780.

[24] W. E. Farneth, R. J. Gorte, *Chemical Reviews* **1995**, *95*, 615-635.

[25] J. Védrine, *Research on Chemical Intermediates* **2015**, 1-37.

[26] J. Macht, R. T. Carr, E. Iglesia, *Journal of Catalysis* **2009**, *264*, 54-66.

[27] R. T. Carr, M. Neurock, E. Iglesia, *Journal of Catalysis* **2011**, *278*, 78-93.
[28] C.-M. Wang, R. Y. Brogaard, B. M. Weckhuysen, J. K. Nørskov, F. Studt, *The Journal of Physical Chemistry Letters* **2014**, *5*, 1516-1521.
[29] R. Y. Brogaard, C.-M. Wang, F. Studt, *ACS Catalysis* **2014**, *4*, 4504-4509.
[30] M. Westgård Erichsen, K. De Wispelaere, K. Hemelsoet, S. L. C. Moors, T. Deconinck, M. Waroquier, S. Svelle, V. Van Speybroeck, U. Olsbye, *Journal of Catalysis* **2015**, *328*, 186-196.
[31] J. S. Martinez-Espin, M. Morten, T. V. W. Janssens, S. Svelle, P. Beato, U. Olsbye, *Catalysis Science & Technology* **2017**.
[32] C.-M. Wang, R. Y. Brogaard, Z.-K. Xie, F. Studt, *Catalysis Science & Technology* **2015**.
[33] S. T. Wilson, B. M. Lok, C. A. Messina, T. R. Cannan, E. M. Flanigen, *Journal of the American Chemical Society* **1982**, *104*, 1146-1147.
[34] H. O. Pastore, S. Coluccia, L. Marchese, *Annual Review of Materials Research* **2005**, *35*, 351-395.
[35] B. M. Weckhuysen, R. R. Rao, J. A. Martens, R. A. Schoonheydt, *European Journal of Inorganic Chemistry* **1999**, *1999*, 565-577.
[36] M. Hartmann, L. Kevan, *Chemical Reviews* **1999**, *99*, 635-664.
[37] G. Lischke, B. Parlitz, U. Lohse, E. Schreier, R. Fricke, *Applied Catalysis A: General* **1998**, *166*, 351-361.
[38] S. K. Saha, S. B. Waghmode, H. Maekawa, K. Komura, Y. Kubota, Y. Sugi, Y. Oumi, T. Sano, *Microporous and Mesoporous Materials* **2005**, *81*, 289-303.
[39] S. K. Saha, H. Maekawa, S. B. Waghmode, S. A. R. Mulla, K. Komura, Y. Kubota, Y. Sugi, S. J. Cho, *MATERIALS TRANSACTIONS* **2005**, *46*, 2659-2667.
[40] L. Feng, X. Qi, J. Li, Y. Zhu, L. Zhu, *React Kinet Catal Lett* **2009**, *98*, 327-339.
[41] M. K. Dongare, D. P. Sabde, R. A. Shaikh, K. R. Kamble, S. G. Hegde, *Catalysis Today* **1999**, *49*, 267-276.
[42] O. Kresnawahjuesa, R. J. Gorte, D. de Oliveira, L. Y. Lau, *Catalysis Letters* **2002**, *82*, 155-160.
[43] W. van Beek, O. V. Safonova, G. Wiker, H. Emerich, *Phase Transitions* **2011**, *84*, 726-732.
[44] P. M. Abdala, O. V. Safonova, G. Wiker, W. van Beek, H. Emerich, J. A. van Bokhoven, J. Sá, J. Szlachetko, M. Nachtegaal, *Chimia (Basel)* **2012**, *66*, 699-705.
[45] S. Bordiga, E. Groppo, G. Agostini, J. A. van Bokhoven, C. Lamberti, *Chemical Reviews* **2013**, *113*, 1736-1850.
[46] C. Lamberti, S. Bordiga, D. Arduino, A. Zecchina, F. Geobaldo, G. Spanó, F. Genoni, G. Petrini, A. Carati, F. Villain, G. Vlaic, *The Journal of Physical Chemistry B* **1998**, *102*, 6382-6390.
[47] T. V. W. Janssens, H. Falsig, L. F. Lundegaard, P. N. R. Vennestrøm, S. B. Rasmussen, P. G. Moses, F. Giordanino, E. Borfecchia, K. A. Lomachenko, C. Lamberti, S. Bordiga, A. Godiksen, S. Mossin, P. Beato, *ACS Catalysis* **2015**, *5*, 2832-2845.
[48] K. A. Lomachenko, E. Borfecchia, C. Negri, G. Berlier, C. Lamberti, P. Beato, H. Falsig, S. Bordiga, *Journal of the American Chemical Society* **2016**, *138*, 12025-12028.
[49] Y. Tulchinsky, C. H. Hendon, K. A. Lomachenko, E. Borfecchia, B. C. Melot, M. R. Hudson, J. D. Tarver, M. D. Korzyński, A. W. Stubbs, J. J. Kagan, C. Lamberti, C. M. Brown, M. Dincă, *Journal of the American Chemical Society* **2017**, *139*, 5992-5997.
[50] M. Westgård Erichsen, S. Svelle, U. Olsbye, *Journal of Catalysis* **2013**, *298*, 94-101.
[51] S. H. Newland, W. Sinkler, T. Mezza, S. R. Bare, R. Raja, *Proceedings of the Royal Society A: Mathematical, Physical and Engineering Science* **2016**, *472*.
[52] F. Corà, C. R. A. Catlow, *The Journal of Physical Chemistry B* **2001**, *105*, 10278-10281.
[53] G. Müller, J. Bódis, G. Eder-Mirth, J. Kornatowski, J. A. Lercher, *Journal of Molecular Structure* **1997**, *410*, 173-178.
[54] J. Chen, J. M. Thomas, G. Sankar, *Journal of the Chemical Society, Faraday Transactions* **1994**, *90*, 3455-3459.
[55] J. Janchen, M. P. J. Peeters, J. H. M. C. van Wolput, J. P. Wolthuizen, J. H. C. van Hooff, U. Lohse, *Journal of the Chemical Society, Faraday Transactions* **1994**, *90*, 1033-1039.

[56] I. Kustanovich, D. Goldfarb, *The Journal of Physical Chemistry* **1991**, *95*, 8818-8823.
[57] M. Popova, C. Minchev, V. Kanazirev, *React Kinet Catal Lett* **1998**, *63*, 379-384.
[58] Z. Wei, Y.-Y. Chen, J. Li, P. Wang, B. Jing, Y. He, M. Dong, H. Jiao, Z. Qin, J. Wang, W. Fan, *Catalysis Science & Technology* **2016**, *6*, 5526-5533.
[59] J. S. Martinez-Espin, K. De Wispelaere, M. Westgård Erichsen, S. Svelle, T. V. W. Janssens, V. Van Speybroeck, P. Beato, U. Olsbye, *Journal of Catalysis* **2017**, *349*, 136-148.
[60] W. Dai, W. Kong, G. Wu, N. Li, L. Li, N. Guan, *Catalysis Communications* **2011**, *12*, 535-538.
[61] S. Teketel, M. Westgard Erichsen, F. Lonstad Bleken, S. Svelle, K. Petter Lillerud, U. Olsbye, in *Catalysis: Volume 26, Vol. 26*, The Royal Society of Chemistry, **2014**, pp. 179-217.
[62] D. M. McCann, D. Lesthaeghe, P. W. Kletnieks, D. R. Guenther, M. J. Hayman, V. Van Speybroeck, M. Waroquier, J. F. Haw, *Angewandte Chemie International Edition* **2008**, *47*, 5179-5182.
[63] M. Westgård Erichsen, M. Mortén, S. Svelle, O. Sekiguchi, E. Uggerud, U. Olsbye, *ChemCatChem* **2015**, n/a-n/a.
[64] L. Lin, C. Qiu, Z. Zhuo, D. Zhang, S. Zhao, H. Wu, Y. Liu, M. He, *Journal of Catalysis* **2014**, *309*, 136-145.
[65] L. F. Lin, S. F. Zhao, D. W. Zhang, H. Fan, Y. M. Liu, M. Y. He, *ACS Catalysis* **2015**, *5*, 4048-4059.
[66] J. Meusinger, H. Vinek, J. A. Lercher, *Journal of Molecular Catalysis* **1994**, *87*, 263-273.
[67] Y. V. Kissin, *Catalysis Reviews* **2001**, *43*, 85-146.
[68] D. A. Simonetti, J. H. Ahn, E. Iglesia, *Journal of Catalysis* **2011**, *277*, 173-195.
[69] Y. Liu, S. Müller, D. Berger, J. Jelic, K. Reuter, M. Tonigold, M. Sanchez-Sanchez, J. A. Lercher, *Angewandte Chemie International Edition* **2016**, *55*, 5723-5726.
[70] S. Müller, Y. Liu, M. Vishnuvarthan, X. Sun, A. C. van Veen, G. L. Haller, M. Sanchez-Sanchez, J. A. Lercher, *Journal of Catalysis* **2015**, *325*, 48-59.
[71] H. Schulz, *Catalysis Today* **2010**, *154*, 183-194.
[72] R. Bulánek, K. Novoveská, B. Wichterlová, *Applied Catalysis A: General* **2002**, *235*, 181-191.
[73] C. O. Arean, M. R. Delgado, P. Nachtigall, H. V. Thang, M. Rubes, R. Bulanek, P. Chlubna-Eliasova, *Physical Chemistry Chemical Physics* **2014**, *16*, 10129-10141.
[74] F. Bleken, M. Bjørgen, L. Palumbo, S. Bordiga, S. Svelle, K.-P. Lillerud, U. Olsbye, *Top Catal* **2009**, *52*, 218-228.